Arch. Mech., **51**, 3–4, pp. 419–446, Warszawa 1999

Stiffness degradation in gradient-dependent coupled damage-plasticity

J. PAMIN[1)] and R. de BORST

Koiter Institute Delft, Faculty of Aerospace Engineering,
Delft University of Technology,
P.O. Box 5058, 2600 GB Delft, the Netherlands,
e-mail R.deBorst@lr.TUDelft.nl

TWO GRADIENT-DEPENDENT COMBINATIONS of isotropic plasticity and scalar damage are proposed. The gradient enhancements of either the plasticity or the damage component of the theory are performed by introducing the Laplacian of a strain measure and an internal length parameter. This makes the constitutive models applicable to localization analyses. The models are used for finite element simulations of localization in a one-dimensional tensile bar problem. The coupling of hardening/softening plasticity with damage governed by different damage evolution functions is discussed. Then, attention is focused on the response of the models in unloading from localized deformation states. The model of gradient damage combined with hardening plasticity is used to predict progressive damage of concrete in a beam subjected to four-point bending. The simulated stiffness degradation is compared with experimental results.

Keywords: gradient-dependent continuum, plasticity, damage, strain localization, finite elements

1. Introduction

IN A PHENOMENOLOGICAL CONSTITUTIVE description, a combination of plasticity and damage theories is physically appealing since a host of materials exhibit an interaction of inelastic mechanisms of microcrack or microvoid growth with plastic flow. The coupled models make it possible to reproduce a realistic elastic stiffness degradation, which is crucial for cyclic loading and extensive stress redistributions.

The research on the incorporation of elastic stiffness degradation within the theory of plasticity goes back to the works [1, 2, 3, 4, 5]. Confining interest to

[1)] on leave from Faculty of Civil Engineering, Cracow University of Technology, Cracow, Poland

small strain theories, plasticity and damage combinations have been considered amongst others in [6, 7, 8, 9, 10, 11], although they all restricted themselves to a local continuum form.

In quasi-brittle materials the inelastic behaviour is accompanied by localization of deformation and progressive fracture. The problem of localization, driven by material instabilities like strain softening, has recently been thoroughly investigated, see for instance [12] and references therein. Within a classical, local continuum formulation this phenomenon is associated with the loss of well-posedness of the governing partial differential equations, and therefore discretization methods used to solve them may give mesh-sensitive results. To overcome this problem, some form of nonlocal or rate-dependent enhancement of the constitutive model must be adopted [13, 14, 15]. In other words, a continuum formulation should be equipped with an internal length parameter.

This paper investigates the damage evolution and the resulting elastic stiffness degradation using gradient-enhanced plastic-damage theories. The coupling of plasticity and damage is based on the effective stress concept and strain equivalence [7, 8]. However, a gradient enhancement of either plasticity or damage has been adopted [16, 17]. The gradient-dependent plasticity enhancement is based on [18, 19, 20]. The gradient damage model follows [21, 22]. A gradient-regularized hardening plasticity theory has so far been coupled to damage in [23].

The numerical response of the gradient-dependent coupled plasticity-damage models in localization problems involving load reversals is examined. Although the models are general, consideration is focused on the tensile regime. Section 2 summarizes the adopted plasticity-damage theory. In Sections 3 and 4 the two gradient-enhanced constitutive models are presented [17]. In Section 5 the employed equivalent strain measures and damage evolution laws are discussed. Section 6 presents the results of one-dimensional numerical studies. Section 7 contains some simulations of damage and stiffness degradation in a notched concrete beam subjected to four-point bending. Final remarks are gathered in Section 8.

2. Coupling of local damage and plasticity theories

In the following we assume that configurations are loaded quasi-statically and exhibit small strains, which is usually realistic for quasi-brittle materials. Hence, the equilibrium and kinematic equations have the form:

$$\mathbf{L}^{\mathrm{T}}\boldsymbol{\sigma} + \mathbf{b} = \mathbf{0}, \tag{2.1}$$

$$\boldsymbol{\epsilon} = \mathbf{L}\mathbf{u}, \tag{2.2}$$

where $\mathbf{L}$ is a differential operator matrix, $\boldsymbol{\sigma}$ is the stress tensor in a vector form, $\mathbf{b}$ is the body force vector, $\boldsymbol{\epsilon}$ is the strain tensor in a vector form, $\mathbf{u}$ is the

displacement vector and the superscript T is the transpose symbol. The stresses and displacements satisfy the relevant natural and essential boundary conditions, respectively.

We start the discussion of constitutive relations by selecting a form of coupling between plasticity and damage theories. We combine a plasticity theory formulated in stress space and a damage theory formulated in strain space. The theories have a simple, isotropic format (intrinsic and induced anisotropy is neglected). However, as will be shown in the next sections, one of the two theories is made gradient-dependent [17] in order to assure that numerical simulations of strain localization give meaningful results.

Considering the damage evolution, we distinguish the actual body with strains $\boldsymbol{\epsilon}$ and stresses $\boldsymbol{\sigma}$ and its fictitious undamaged counterpart with stresses $\hat{\boldsymbol{\sigma}}$ and strains $\hat{\boldsymbol{\epsilon}}$. The fictitious counterpart represents the undamaged "skeleton" of the body, and the stresses $\hat{\boldsymbol{\sigma}}$ acting on it are called effective. We adopt the postulate that the strains observed in the actual body and in its undamaged representation are equal [7, 8]:

$$\boldsymbol{\epsilon} = \hat{\boldsymbol{\epsilon}}, \tag{2.3}$$

and that the stresses are related by means of a scalar damage measure ω

$$\boldsymbol{\sigma} = (1 - \omega)\hat{\boldsymbol{\sigma}}. \tag{2.4}$$

The damage ω is a function of a damage history parameter κ^{d} that will be specified below:

$$\omega = \omega(\kappa^{\mathrm{d}}). \tag{2.5}$$

It grows from zero to one as κ^{d} grows from a damage threshold κ_0 to an ultimate value κ_{u}.

Next, we define a damage function which limits the elastic (or elasto-plastic) behaviour of the material in the strain space:

$$f^{\mathrm{d}} = \tilde{\epsilon} - \kappa^{\mathrm{d}} = 0, \tag{2.6}$$

where $\tilde{\epsilon}$ is an equivalent strain measure. During the damage evolution the history parameter κ^{d} is equal to the largest value of $\tilde{\epsilon}$ reached in the loading history. Suitable loading/unloading conditions complete the formulation of the scalar damage model:

$$\dot{\kappa}^{\mathrm{d}} \geqslant 0\,, \quad f^{\mathrm{d}} \leqslant 0\,, \qquad \dot{\kappa}^{\mathrm{d}} f^{\mathrm{d}} = 0, \tag{2.7}$$

where the superposed dot denotes the rate of a quantity.

Although damage and plastic processes can be coupled, plastic flow occurs in the undamaged skeleton of the body, so we can write the elastic constitutive relation between the effective stresses and elastic strains as follows:

$$\hat{\boldsymbol{\sigma}} = \mathbf{D}^{\mathrm{e}}\boldsymbol{\epsilon}^{\mathrm{e}}, \tag{2.8}$$

where $\mathbf{D}^{\mathrm{e}}$ is the elastic stiffness operator. Combining Eqs. (2.4) and (2.8) we obtain the relation:

$$\boldsymbol{\sigma} = (1-\omega)\mathbf{D}^{\mathrm{e}}\boldsymbol{\epsilon}^{\mathrm{e}}, \tag{2.9}$$

in which the damage measure ω accounts for the degradation of the elastic stiffness. Damage does not grow during unloading, so that for a pure damage model the constant (secant) stiffness $(1-\omega)\mathbf{D}^{\mathrm{e}}$ results in unloading to the origin, i.e. no residual strains remain after unloading, which means that microcracks and microvoids are assumed to close completely. The motivation for coupling the model with plasticity is thus to incorporate irreversible strains.

The plastic component of the coupled model is formulated in the effective stress space. The yield condition is as follows

$$f^{\mathrm{p}} = \tilde{\sigma}(\hat{\boldsymbol{\sigma}}) - \sigma_{\mathrm{y}}(\kappa^{\mathrm{p}}) = 0, \tag{2.10}$$

where $\tilde{\sigma}$ is an equivalent stress function, σ_{y} is the yield strength and isotropic hardening is assumed. The yield function satisfies the Kuhn-Tucker conditions:

$$\dot{\lambda} \geqslant 0\,,\ f^{\mathrm{p}} \leqslant 0\,, \qquad \dot{\lambda} f^{\mathrm{p}} = 0, \tag{2.11}$$

in which λ is the plastic multiplier. For simplicity, the equivalence of the plastic multiplier λ and the plastic strain measure κ^{p} is adopted, but extension of the theory to cases where λ and κ^{p} are not equal is straightforward.

The plastic multiplier determines the magnitude of plastic strains according to the classical flow rule, which may be non-associated. Assuming the standard additive decomposition of strain rates into an elastic and a plastic part, the elastic strain rate can be written as:

$$\dot{\boldsymbol{\epsilon}}^{\mathrm{e}} = \dot{\boldsymbol{\epsilon}} - \dot{\lambda}\mathbf{m}(\hat{\boldsymbol{\sigma}}), \tag{2.12}$$

where $\mathbf{m}$ is the plastic flow direction vector in the effective stress space.

Next, we invoke the local plastic consistency condition $\dot{f}^{\mathrm{p}} = 0$ in order to compute $\dot{\lambda}$ and substitute it into Eq. (2.12) to obtain:

$$\dot{\boldsymbol{\epsilon}}^{\mathrm{e}} = \dot{\boldsymbol{\epsilon}} - \frac{1}{h}\mathbf{m}\mathbf{n}^{\mathrm{T}}\dot{\hat{\boldsymbol{\sigma}}}, \tag{2.13}$$

where the classical definitions of the gradient $\mathbf{n}$ normal to the yield function and the softening modulus h are used:

$$\mathbf{n}^{T}(\hat{\boldsymbol{\sigma}}) = \frac{\partial\tilde{\sigma}}{\partial\hat{\boldsymbol{\sigma}}}\,, \qquad h = \frac{\mathrm{d}\sigma_{\mathrm{y}}}{\mathrm{d}\kappa^{\mathrm{p}}}. \tag{2.14}$$

After some rearrangements and with the help of Sherman-Morrison formula, we obtain the tangential relation:

$$\dot{\hat{\sigma}} = \mathbf{D}^{\mathrm{ep}}\dot{\boldsymbol{\epsilon}}, \tag{2.15}$$

with the classical elasto-plastic matrix

$$\mathbf{D}^{\mathrm{ep}} = \mathbf{D}^{\mathrm{e}} - \frac{\mathbf{D}^{\mathrm{e}}\mathbf{m}\mathbf{n}^{\mathrm{T}}\mathbf{D}^{\mathrm{e}}}{h + \mathbf{n}^{\mathrm{T}}\mathbf{D}^{\mathrm{e}}\mathbf{m}}. \tag{2.16}$$

This tangent operator is valid during loading, and the unloading process for the pure plasticity model is completely elastic.

The effective stress rate during the evolution of damage and plasticity can also be obtained by differentiating Eq. (2.8):

$$\dot{\hat{\sigma}} = \mathbf{D}^{\mathrm{e}}\dot{\boldsymbol{\epsilon}}^{\mathrm{e}}, \tag{2.17}$$

and the stress rate can be computed by differentiating Eq. (2.9):

$$\dot{\boldsymbol{\sigma}} = (1-\omega)\,\mathbf{D}^{\mathrm{e}}\dot{\boldsymbol{\epsilon}}^{\mathrm{e}} - \dot{\omega}\,\hat{\boldsymbol{\sigma}}, \tag{2.18}$$

where $\dot{\boldsymbol{\epsilon}}^{\mathrm{e}}$ follows from Eq. (2.12) and the rate of damage during evolution ($\kappa^{\mathrm{d}} = \tilde{\epsilon}$) is computed as:

$$\dot{\omega} = \frac{\partial\omega}{\partial\kappa^{\mathrm{d}}}\frac{\partial\tilde{\epsilon}}{\partial\boldsymbol{\epsilon}}\,\dot{\boldsymbol{\epsilon}}. \tag{2.19}$$

During unloading we have $\dot{\omega} = 0$. Comparing Eq. (2.17) and Eq. (2.15) and using the following definitions:

$$H = \frac{\mathrm{d}\omega}{\mathrm{d}\kappa^{\mathrm{d}}}, \qquad \mathbf{s}^{\mathrm{T}} = \frac{\partial\tilde{\epsilon}}{\partial\boldsymbol{\epsilon}}, \tag{2.20}$$

we obtain the linearized constitutive relation for the coupled model:

$$\dot{\boldsymbol{\sigma}} = [(1-\omega)\,\mathbf{D}^{\mathrm{ep}} - H\hat{\boldsymbol{\sigma}}\,\mathbf{s}^{\mathrm{T}}]\,\dot{\boldsymbol{\epsilon}}. \tag{2.21}$$

3. Gradient plasticity coupled to damage

Now, we revisit the gradient plasticity formulation [18, 19] and write the yield function, which depends on the Laplacian of an equivalent plastic strain measure κ^{p}, in the effective stress space:

$$f^{\mathrm{p}} = \tilde{\sigma}(\hat{\boldsymbol{\sigma}}) - \sigma_{\mathrm{y}}(\kappa^{\mathrm{p}}) + g\nabla^2\kappa^{\mathrm{p}} = 0, \tag{3.1}$$

where $\tilde{\sigma}$ is a classical (e.g. Huber-von Mises or Rankine) yield function and g is a positive gradient influence factor. The yield function satisfies the Kuhn-Tucker

conditions (2.11), but it is now a partial differential equation which must be solved simultaneously with the equilibrium equations.

The enhancement of the classical theory was made in order to preserve well-posedness of the governing equations for materials which do not comply with the material stability requirement [24], e.g. when a softening relation between stresses and strains is assumed ($h < 0$). For a softening medium the factor g can be associated with an internal length parameter l, e.g. in a one-dimensional analytical solution we have $g = -hl^2 > 0$ [19]. However, also for a hardening material the Laplacian term with $g > 0$ regularizes the solution [20] in the sense that a higher-order continuity of the strain field is obtained.

The finite element implementation is based on the following two weak-form equations governing the static equilibrium and the plastic consistency, respectively:

$$\int_V (\mathbf{L}\mathbf{v})^{\mathrm{T}}\boldsymbol{\sigma}\,\mathrm{d}V = \int_V \mathbf{v}^{\mathrm{T}}\mathbf{b}\,\mathrm{d}V + \int_S \mathbf{v}^{\mathrm{T}}\mathbf{t}\,\mathrm{d}S,$$

(3.2)

$$\int_V w\, f^{\mathrm{p}}(\hat{\sigma}, \lambda, \nabla^2\lambda)\mathrm{d}V = 0\,,$$

where $\mathbf{v}$ and w are suitable weighted functions, $\mathbf{t}$ is the traction vector. Equation $(3.2)_2$, which requires the discretization of the λ field, refers to the effective stress space and therefore does not change in presence of damage.

Equations (3.2) are written for iteration $i+1$ of the incremental-iterative algorithm and the following decomposition is used:

$$\boldsymbol{\sigma}^{(i+1)} = \boldsymbol{\sigma}^{(i)} + \mathrm{d}\boldsymbol{\sigma}\,, \quad \lambda^{(i+1)} = \lambda^{(i)} + \mathrm{d}\lambda, \tag{3.3}$$

so that the yield function can be developed in a truncated Taylor series around $(\hat{\boldsymbol{\sigma}}^{(i)}, \lambda^{(i)})$. We obtain the following incremental equations:

$$\int_V (\mathbf{L}\mathbf{v})^{\mathrm{T}}\mathrm{d}\boldsymbol{\sigma}\,\mathrm{d}V = f_{\mathrm{ext}} - f_{\mathrm{int}},$$

(3.4)

$$\int_V w\,[\mathbf{n}^{\mathrm{T}}\mathrm{d}\hat{\boldsymbol{\sigma}} - h\,\mathrm{d}\lambda + g\nabla^2(\mathrm{d}\lambda)]\,\mathrm{d}V = -\int_V w\, f^{\mathrm{p}}(\hat{\boldsymbol{\sigma}}^{(i)}, \kappa^{\mathrm{p}(i)}, \nabla^2\kappa^{\mathrm{p}(i)})\,\mathrm{d}V,$$

with

$$f_{\mathrm{ext}} = \int_S \mathbf{v}^{\mathrm{T}}\mathbf{t}\,\mathrm{d}S + \int_V \mathbf{v}^{\mathrm{T}}\mathbf{b}\,\mathrm{d}V,$$

(3.5)

$$f_{\mathrm{int}} = \int_V (\mathbf{L}\mathbf{v})^{\mathrm{T}}\boldsymbol{\sigma}^{(i)}\,\mathrm{d}V.$$

It is important to notice that, if the yield condition (3.1) is used in the classical return mapping algorithm to distinguish between elastic and plastic states, a C^1-continuous interpolation of λ is unavoidable, otherwise $\nabla^2\lambda$ loses its meaning [20]. Therefore, the Laplacian term is not removed from the left-hand side of Eq. $(3.4)_2$, although this can be done using Green's formula if a homogeneous non-standard boundary condition $(\nabla \mathrm{d}\lambda)^{\mathrm{T}}\boldsymbol{\nu} = 0$ is assumed ($\boldsymbol{\nu}$ is a vector normal to the surface of the plastic part of the body).

Next, we substitute Eq. (2.12) into Eqs. (2.18) and (2.17) and substitute their incremental forms into Eqs. $(3.4)_1$ and $(3.4)_2$, respectively:

$$\begin{aligned}
&\int_V (\mathbf{L}\mathbf{v})^{\mathrm{T}}[(1-\omega^{(i)})\mathbf{D}^{\mathrm{e}}\mathrm{d}\boldsymbol{\epsilon} - \hat{\boldsymbol{\sigma}}^{(i)}\mathrm{d}\omega]\,\mathrm{d}V \\
&\qquad - \int_V (\mathbf{L}\mathbf{v})^{\mathrm{T}}[(1-\omega^{(i)})\mathbf{D}^{\mathrm{e}}\mathbf{m}^{(i)}\,\mathrm{d}\lambda]\,\mathrm{d}V = f_{\mathrm{ext}} - f_{\mathrm{int}}, \\
&\int_V w\,\mathbf{n}^{\mathrm{T}(i)}\mathbf{D}^{\mathrm{e}}\mathrm{d}\boldsymbol{\epsilon}\,\mathrm{d}V - \int_V w\,[(h^{(i)} + \mathbf{n}^{\mathrm{T}(i)}\mathbf{D}^{\mathrm{e}}\mathbf{m}^{(i)})\mathrm{d}\lambda + g\nabla^2(\mathrm{d}\lambda)]\,\mathrm{d}V \\
&\qquad = -\int_V w\,f^{\mathrm{p}}(\hat{\boldsymbol{\sigma}}^{(i)}, \kappa^{\mathrm{p}(i)}, \nabla^2\kappa^{\mathrm{p}(i)})\,\mathrm{d}V.
\end{aligned} \tag{3.6}$$

The increment of damage $\mathrm{d}\omega$ is non-zero only when damage grows, i.e. when Eq. (2.6) is satisfied. With the definitions in Eq. (2.20) it can be related to the strain increment:

$$\mathrm{d}\omega = H\,\mathbf{s}^{\mathrm{T}}\mathrm{d}\boldsymbol{\epsilon}. \tag{3.7}$$

Substituting Eq. (3.7) into Eq. $(3.6)_1$ and defining the elastic-damage tangent operator as:

$$\mathbf{D}^{\mathrm{ed}} = (1-\omega^{(i)})\mathbf{D}^{\mathrm{e}} - H^{(i)}\,\hat{\boldsymbol{\sigma}}^{(i)}\mathbf{s}^{\mathrm{T}(i)} \tag{3.8}$$

we obtain the following final form of Eqs. (3.6):

$$\begin{aligned}
&\int_V (\mathbf{L}\mathbf{v})^{\mathrm{T}}\mathbf{D}^{\mathrm{ed}}\mathrm{d}\boldsymbol{\epsilon}\,\mathrm{d}V - \int_V (\mathbf{L}\mathbf{v})^{\mathrm{T}}[(1-\omega^{(i)})\mathbf{D}^{\mathrm{e}}\mathbf{m}^{(i)}\,\mathrm{d}\lambda]\,\mathrm{d}V = f_{\mathrm{ext}} - f_{\mathrm{int}}, \\
&\int_V w\,\mathbf{n}^{\mathrm{T}(i)}\mathbf{D}^{\mathrm{e}}\mathrm{d}\boldsymbol{\epsilon}\,\mathrm{d}V - \int_V w\,[(h^{(i)} + \mathbf{n}^{\mathrm{T}(i)}\mathbf{D}^{\mathrm{e}}\mathbf{m}^{(i)})\mathrm{d}\lambda + g\nabla^2(\mathrm{d}\lambda)]\,\mathrm{d}V \\
&\qquad = -\int_V w\,f^{\mathrm{p}}(\hat{\boldsymbol{\sigma}}^{(i)}, \kappa^{\mathrm{p}(i)}, \nabla^2\kappa^{\mathrm{p}(i)})\,\mathrm{d}V.
\end{aligned} \tag{3.9}$$

Details of the finite element implementation can be found in [17].

4. Gradient damage coupled to isotropic plasticity

In the second formulation the plasticity theory remains standard and the damage theory is made nonlocal. It is emphasized that in this combination, the unstable material behaviour is caused by damage, and the plasticity model (for instance Huber-von Mises or Drucker-Prager plasticity) is hardening.

Following [21], the damage evolution is now governed by the following damage loading function:

$$f^{\mathrm{d}} = \bar{\epsilon} - \kappa^{\mathrm{d}} = 0, \tag{4.1}$$

where the averaged (nonlocal) strain measure $\bar{\epsilon}$ satisfies the Helmholtz equation:

$$\bar{\epsilon} - c\nabla^2\bar{\epsilon} = \tilde{\epsilon}. \tag{4.2}$$

The loading/unloading conditions (2.7) still apply. The parameter $c > 0$ has a unit of length squared and is hence related to an internal length scale. It is assumed here to be constant, although, with some modifications in the formulation, it can be made a function of $\tilde{\epsilon}$ or $\bar{\epsilon}$ [22].

The finite element implementation is based on the equilibrium Eq. $(3.2)_1$ and a weak form of Eq. (4.2) obtained using Green's formula and the non-standard boundary condition $(\nabla\bar{\epsilon})^{\mathrm{T}}\mathbf{n} = 0$:

$$\int_V [w\bar{\epsilon} + c(\nabla w)^{\mathrm{T}}\nabla\bar{\epsilon}]\mathrm{d}V = \int_V w\,\tilde{\epsilon}\mathrm{d}V. \tag{4.3}$$

In the ensuing two-field formulation the average strain measure must be discretized in addition to the displacements, but C^0-continuity now suffices for all shape functions. The coupling to plasticity influences only the equilibrium Eq. $(3.2)_1$, while Eq. (4.3) is exactly the same as for pure gradient damage.

We write Eqs. $(3.2)_1$ and (4.3) for iteration $i+1$ of the incremental-iterative algorithm and decompose the stress vector, the strain measure and its averaged version as

$$\boldsymbol{\sigma}^{(i+1)} = \boldsymbol{\sigma}^{(i)} + \mathrm{d}\boldsymbol{\sigma}\,, \qquad \tilde{\epsilon}^{(i+1)} = \tilde{\epsilon}^{(i)} + \mathrm{d}\tilde{\epsilon}\,, \qquad \bar{\epsilon}^{(i+1)} = \bar{\epsilon}^{(i)} + \mathrm{d}\bar{\epsilon} \tag{4.4}$$

to obtain:

$$\begin{aligned} \int_V (\mathbf{L}\mathbf{v})^{\mathrm{T}}\mathrm{d}\boldsymbol{\sigma}\,\mathrm{d}V &= f_{\mathrm{ext}} - f_{\mathrm{int}} \\ &\quad - \int_V w\,\mathrm{d}\tilde{\epsilon}\,\mathrm{d}V + \int_V [w\,\mathrm{d}\bar{\epsilon} + c(\nabla w)^{\mathrm{T}}\nabla(\mathrm{d}\bar{\epsilon})]\,\mathrm{d}V \\ &= \int_V w\,\tilde{\epsilon}^{(i)}\,\mathrm{d}V - \int_V [w\bar{\epsilon}^{(i)} + c(\nabla w)^{\mathrm{T}}\nabla\bar{\epsilon}^{(i)}]\,\mathrm{d}V. \end{aligned} \tag{4.5}$$

Equation (2.21) is now invoked in an incremental form:

$$\mathrm{d}\boldsymbol{\sigma} = (1-\omega)\mathbf{D}^{\mathrm{ep}}\mathrm{d}\boldsymbol{\epsilon} - \mathrm{d}\omega\hat{\boldsymbol{\sigma}}, \tag{4.6}$$

and, when Eq. (4.1) holds, the damage increment $\mathrm{d}\omega$ can be computed as

$$\mathrm{d}\omega = H\mathrm{d}\bar{\epsilon}, \tag{4.7}$$

with H defined in Eq. $(2.20)_1$. The increment of strain measure $\mathrm{d}\bar{\epsilon}$ is computed as:

$$\mathrm{d}\bar{\epsilon} = \mathbf{s}^{\mathrm{T}}\mathrm{d}\boldsymbol{\epsilon}, \tag{4.8}$$

with $\mathbf{s}^{\mathrm{T}}$ defined in Eq. $(2.20)_2$. Equation (4.7) is substituted into Eq. (4.6) and next Eqs. (4.6) and (4.8) are substituted into Eqs. $(4.5)_1$ and $(4.5)_2$, respectively, to obtain:

$$\begin{aligned} &\int_V (\mathbf{Lv})^{\mathrm{T}}(1-\omega^{(i)})\mathbf{D}^{\mathrm{ep}}\mathrm{d}\boldsymbol{\epsilon}\,\mathrm{d}V - \int_V (\mathbf{Lv})^{\mathrm{T}}H^{(i)}\hat{\boldsymbol{\sigma}}^{(i)}\mathrm{d}\bar{\epsilon}\,\mathrm{d}V = f_{\mathrm{ext}} - f_{\mathrm{int}} \\ &- \int_V w\,\mathbf{s}^{\mathrm{T}(i)}\mathrm{d}\boldsymbol{\epsilon}\,\mathrm{d}V + \int_V [w\,\mathrm{d}\bar{\epsilon} + c(\nabla w)^{\mathrm{T}}\nabla(\mathrm{d}\bar{\epsilon})]\,\mathrm{d}V \\ &= \int_V w\,\bar{\epsilon}^{(i)}\,\mathrm{d}V - \int_V [w\,\bar{\epsilon}^{(i)} + c(\nabla w)^{\mathrm{T}}\nabla\bar{\epsilon}^{(i)}]\,\mathrm{d}V. \end{aligned} \tag{4.9}$$

In fact, a similar matrix form of incremental equations is obtained upon discretization for both combinations of the local and gradient-dependent theories, leading to two-field mixed finite elements. Further details of the numerical implementation, consistent linearization and other algorithmic aspects can be found in [17].

5. Equivalent strain measures and damage laws

So far, the equivalent strain measure $\tilde{\epsilon}$ has been left unspecified. It can be defined as the damage energy release rate, cf. [8], or a modified form thereof which satisfies the condition that for a uniaxial strain $\tilde{\epsilon} = |\epsilon|$:

$$\tilde{\epsilon} = \sqrt{\frac{1}{E}\boldsymbol{\epsilon}^{\mathrm{T}}\mathbf{D}^{\mathrm{e}}\boldsymbol{\epsilon}}, \tag{5.1}$$

where E is Young's modulus. For quasi-brittle materials a more suitable form, taking into account the difference between the tensile and compressive strength,

can be adopted [25, 26], e.g. the modified von Mises definition of the equivalent strain measure [26], which has been used here:

$$\tilde{\epsilon} = \frac{k-1}{2k(1-2\nu)} I_1 + \frac{1}{2k}\sqrt{\left(\frac{k-1}{1-2\nu} I_1\right)^2 + \frac{12k}{(1+\nu)^2} J_2}, \tag{5.2}$$

where k is a ratio of uniaxial compressive and tensile strength, ν is Poisson's ratio, I_1 is the first invariant of the strain tensor and J_2 is the second invariant of the strain deviator. In Fig. 1 this strain measure is compared with the definition in Eq. (5.1). The figure has been plotted for plane-stress conditions, $\tilde{\epsilon} = 0.001$, $k = 10$ and $\nu = 0.2$.

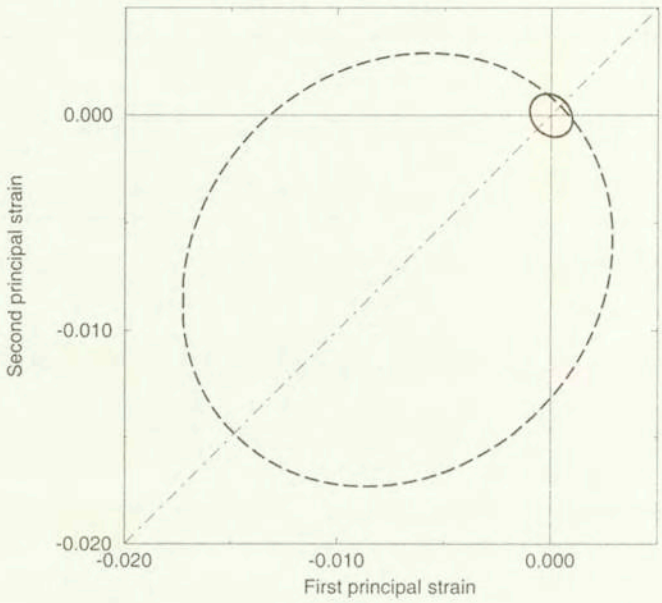

FIG. 1. Comparison of equivalent strain measure definitions: Eq. (5.1) – solid versus Eq. (5.2) – dashed.

Another issue is whether $\tilde{\epsilon}$ should be a measure of total strains, their elastic part or some other function of elastic and plastic strains [8]. If it is assumed that the equivalent strain measure is a function of elastic strains only, $\tilde{\epsilon}(\boldsymbol{\epsilon}^{\mathrm{e}})$, which means that the damage growth is driven by the effective stresses, see Eq. (2.8), the two theories become weakly coupled. If a full coupling exists, for instance for plastically induced damage in metals, plastic strains should also contribute to $\tilde{\epsilon}$.

In this paper, for gradient plasticity combined with damage, $\tilde{\epsilon}$ has been assumed to be an equivalent measure of the total strains $\tilde{\epsilon}(\boldsymbol{\epsilon})$. A measure of elastic strains only obviously loses sense in the case of softening plasticity and, for the

gradient regularization to be active within the considered model, the damage growth should depend on the nonlocal plastic strains. For gradient damage combined with plasticity we consider two possibilities: $\bar{\epsilon}(\boldsymbol{\epsilon})$ and $\bar{\epsilon}(\boldsymbol{\epsilon}^{\mathrm{e}})$. In the latter case the computation of $\mathbf{s}^{\mathrm{T}}$ in Eq. (2.20) becomes slightly more intricate, since it then equals:

$$\mathbf{s}^{\mathrm{T}} = \frac{\mathrm{d}\bar{\epsilon}}{\mathrm{d}\boldsymbol{\epsilon}^{\mathrm{e}}} \frac{\mathrm{d}\boldsymbol{\epsilon}^{\mathrm{e}}}{\mathrm{d}\boldsymbol{\epsilon}} = \frac{\mathrm{d}\bar{\epsilon}}{\mathrm{d}\boldsymbol{\epsilon}^{\mathrm{e}}} (\mathbf{D}^{\mathrm{e}})^{-1} \mathbf{D}^{\mathrm{ep}}. \tag{5.3}$$

The damage growth function (2.5), which governs the stress evolution and elastic stiffness degradation, represents a uniaxial stress-strain relationship. It can be validated by experimental measurements. In this paper we use three different damage growth functions. A linear dependence of ω on κ^{d}:

$$\omega(\kappa^{\mathrm{d}}) = \frac{\kappa^{\mathrm{d}} - \kappa_{\mathrm{o}}}{\kappa_{\mathrm{u}} - \kappa_{\mathrm{o}}} \tag{5.4}$$

means that, although eventually the stress drops to zero, there is a hardening stage in the stress-strain relationship. Secondly, the function can represent a linear softening stress-strain diagram:

$$\omega(\kappa^{\mathrm{d}}) = \frac{\kappa_{\mathrm{u}}}{\kappa^{\mathrm{d}}} \frac{\kappa^{\mathrm{d}} - \kappa_{\mathrm{o}}}{\kappa_{\mathrm{u}} - \kappa_{\mathrm{o}}}. \tag{5.5}$$

Case (5.4) will further be called "linear damage", while case (5.5) will just be called "damage". Finally, we will use an exponential damage function which represents exponential softening:

$$\omega(\kappa^{\mathrm{d}}) = 1 - \frac{\kappa_{\mathrm{o}}}{\kappa^{\mathrm{d}}} \left(1 - \alpha + \alpha e^{-\eta(\kappa^{\mathrm{d}} - \kappa_{\mathrm{o}})}\right), \tag{5.6}$$

where α and η are additional parameters. This function is suitable for reproducing the experimental tensile fracture in concrete, since the experimental uniaxial softening relation is exponential [27]. Since it approaches the complete loss of coherence ($\omega = 1$) asymptotically, singularities caused by a complete loss of strength are also avoided.

6. One-dimensional numerical studies

Firstly, implications of the three damage laws are illustrated using a uniaxial problem shown in Fig. 2 and a pure gradient-damage theory. We analyze a bar with a unit cross-section and a geometrical imperfection, subjected to tension. In order to initiate strain localization, a 10% smaller cross-section is adopted in the central zone $d = 10$ mm. Symmetry of deformation is imposed. The length of the bar is $L = 100$ mm, Young's modulus is $E = 20000$ N/mm^2. Eighty

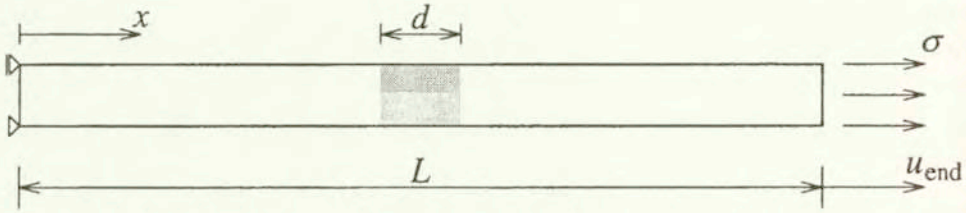

FIG. 2. Tensile bar with imperfection for localization studies.

C^0-continuous three-noded gradient damage elements are used with two-point Gaussian integration [21]. The elements have a quadratic and linear interpolation of the displacement and averaged strain, respectively. A gradient constant $c = 4$ mm^2 is adopted.

In a one-dimensional problems the equivalent strain measure $\tilde{\epsilon}$ is equal to the absolute value of the axial strain ϵ. For all damage laws the same damage threshold $\kappa_0 = 0.0001$ is used. For linear damage, Eq. (5.4), we adopt $\kappa_u = 0.0005$ and for the damage growth function representing linear softening, Eq. (5.5), $\kappa_u = 0.0125$. The exponential damage parameters, Eq. (5.6), are: $\alpha = 1.00$, $\eta = 200$.

Figures 3–4 demonstrate that the response of the model is quite different although the gradient influence factor is the same for all cases. The load-displacement diagrams in Fig. 3 show the computed relations between the stress at the right-hand end of the bar σ and the elongation of the bar u_{end}. For linear damage we first observe a hardening stage and then a severe snap-back behaviour while the originally distributed damage profile in Fig. 3b strongly localizes and damage finally grows only in the smallest possible volume (two integration points).

For the second case (Fig. 4a) the damage zone first broadens and then the points at its boundary gradually enter unloading, which is also accompanied by snap-back behaviour in Fig. 3a. In the final stage the deformation also localizes in the two central integration points. This is because the strain and damage finally localize in a crack at midspan of the bar. Up to this moment, localization is limited during the whole deformation history.

For the exponential law the damage zone in Fig. 4b is narrower, since softening is more pronounced in the first stage of the damage process. However, for this case the bar extension does not exhibit a snap-back and $\omega = 1$ is approached simultaneously in a larger set of central points. The interpretation of a continuous damage evolution into a crack is lost in this case.

The gradient-enhanced coupled theories will now be applied in the uniaxial localization problem from Fig. 2 in order to illustrate the basic properties of the models in loading and unloading. It is noted that mesh sensitivity studies have been presented in [17] and will not be repeated here.

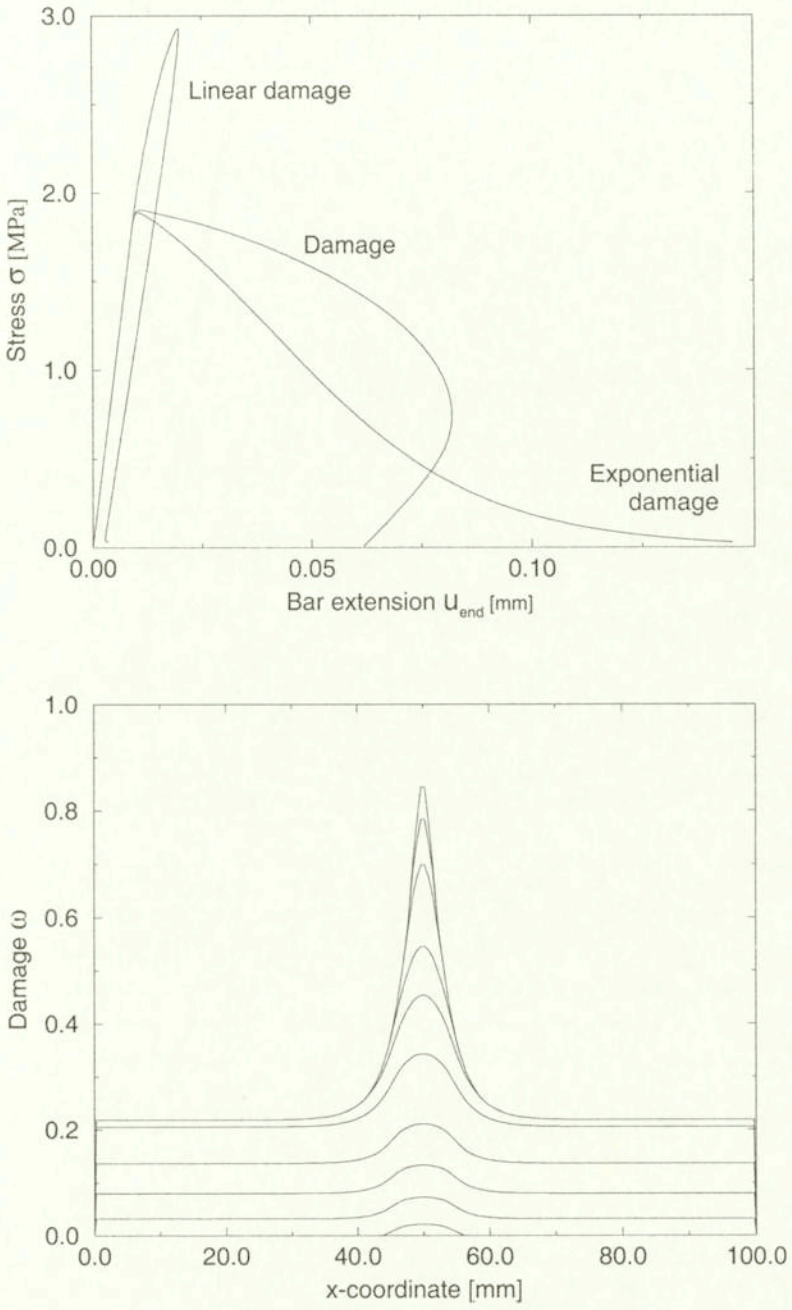

FIG. 3. Comparison of results for different damage growth functions and $c = 4$ mm^2: (a) load-displacement diagrams, (b) damage evolution for linear damage.

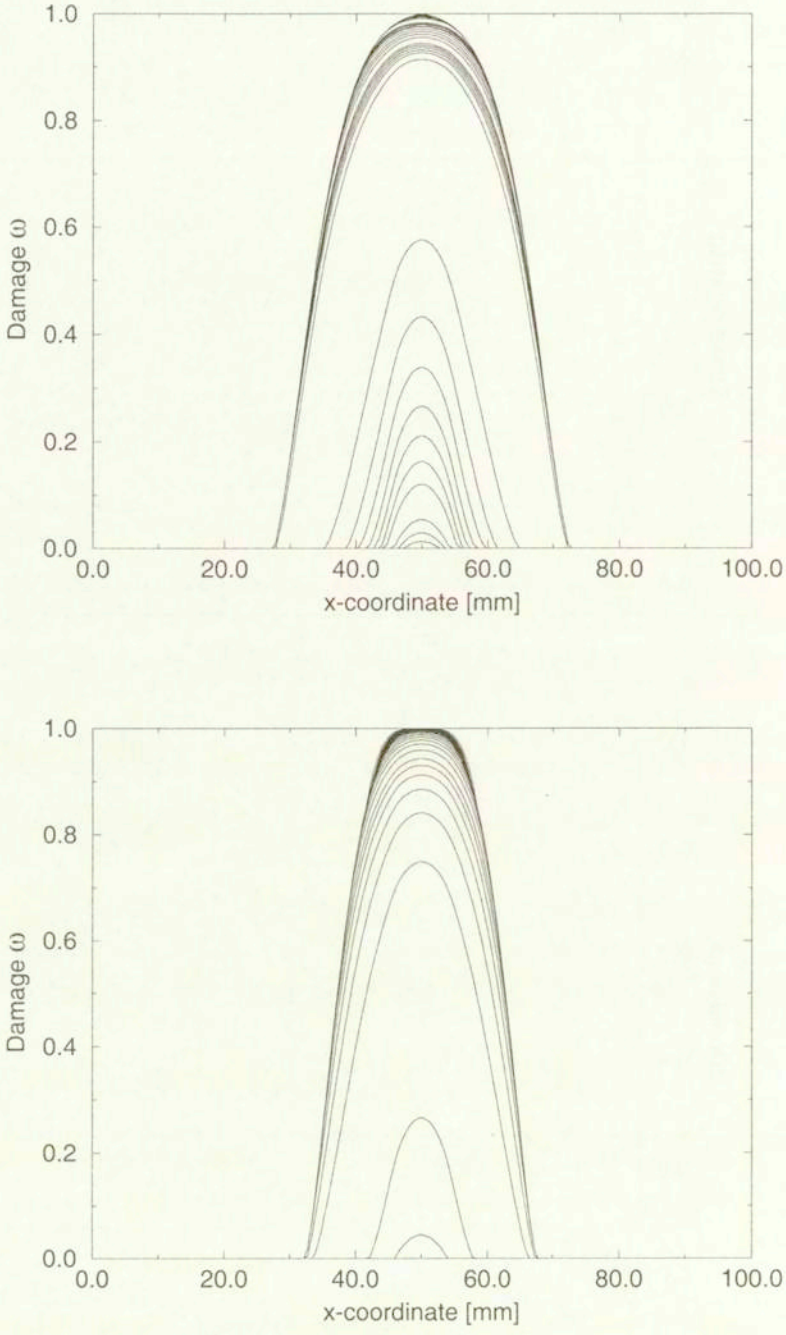

FIG. 4. Damage evolution for $c = 4$ mm^2 and: (a) damage growth function representing linear softening, (b) exponential damage growth function.

6.1. Gradient plasticity coupled to scalar damage

In the uniaxial case the Huber-von Mises or Rankine yield functions give $\tilde{\sigma} = |\sigma|$. The tensile strength is $\sigma_y = 2$ N/mm^2. We employ a discretization with eighty C^1-continuous three-noded gradient plasticity elements [20]. The derivative of the plastic multiplier is set to zero at both ends of the bar to allow for reduced integration.

First, softening gradient plasticity is coupled to damage. Linear softening with $h = -500$ N/mm^2 and the gradient constant $g = 12500$ N are adopted, so that the width of the localization zone predicted by gradient plasticity is $w = 2\pi l = 31.4$ mm [19]. In Fig. 5a the solution obtained for pure gradient plasticity is compared with the coupled model, in which $\bar{\epsilon}$ is the total strain. The damage evolution is activated later than the plastic flow by adopting the damage threshold $\kappa_o = 0.001$. The linear damage with $\kappa_u = 0.01$ and the damage law from Eq. (5.5) with $\kappa_u = 0.1$ are used. For the linear relation $\omega(\kappa^d)$ the damage growth is initially much slower, but the ultimate value $\kappa_u = 0.01$ associated with $\omega = 1$ and $\sigma = 0$ is reached for smaller extension of the bar.

It is observed that the localization zone first expands from the imperfect elements, then its width remains almost constant and, finally, the plastic zone starts to grow again while the load-displacement diagram bends upwards, since in the central points the softening diagram is exited. For pure gradient plasticity the width of the localization zone is equal to the expected value during the linear softening stage. For the coupled model the plastic strains are more localized due to interaction with damage, but a spurious tendency to localize in the smallest possible volume is not observed [17]. Apparently, the gradient regularization is active in spite of adding the second destabilizing component to the constitutive description.

In Fig. 5a unloading branches at some extension levels are also shown. For pure gradient plasticity the unloading is elastic, but, quite surprisingly, also for the coupling to damage the unloading stiffness reduction is very small. The plasticity model dominates.

Secondly, for hardening gradient plasticity, we preserve the gradient constant $g = 12500$ N and we adopt a linear hardening with $h = 500$ N/mm^2. For the linear damage model $\kappa_o = 0.0005$ and $\kappa_u = 0.01$. For the damage growth function representing linear softening $\kappa_u = 0.1$ and two damage thresholds are considered: $\kappa_o = 0.0001$ and $\kappa_o = 0.0005$. For the former case the damage and plastic processes are activated simultaneously, i.e. κ_o is reached for the same load as σ_y. Figure 5b presents the obtained load-displacement diagrams and Fig. 6 gives the damage evolution in the bar.

For the case of pure gradient plasticity or when the onset of the damage process is delayed until after the initiation of plasticity we first observe yielding

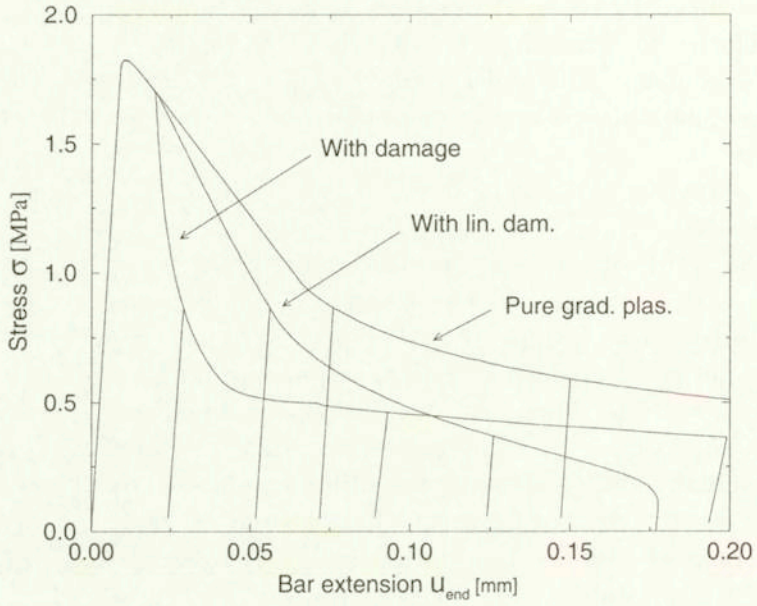

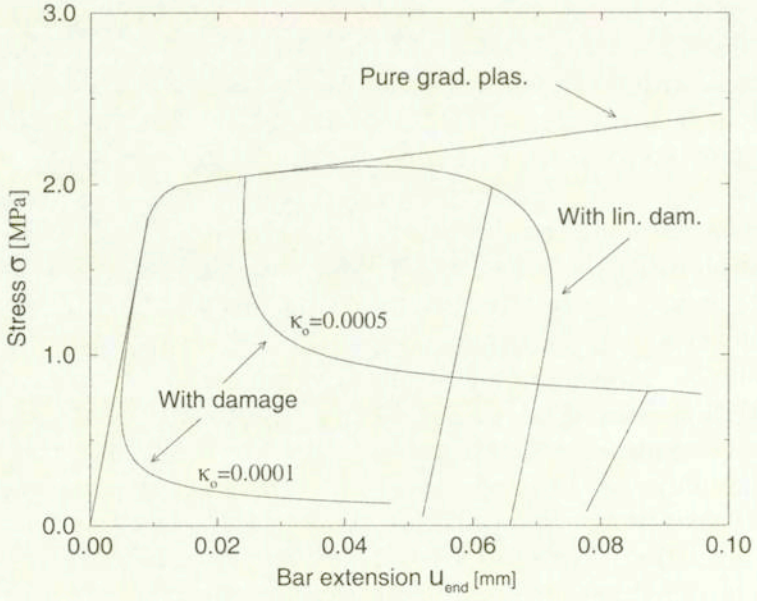

FIG. 5. (a) Load-displacement diagrams for gradient plasticity with damage: (a) softening plasticity, (b) hardening plasticity.

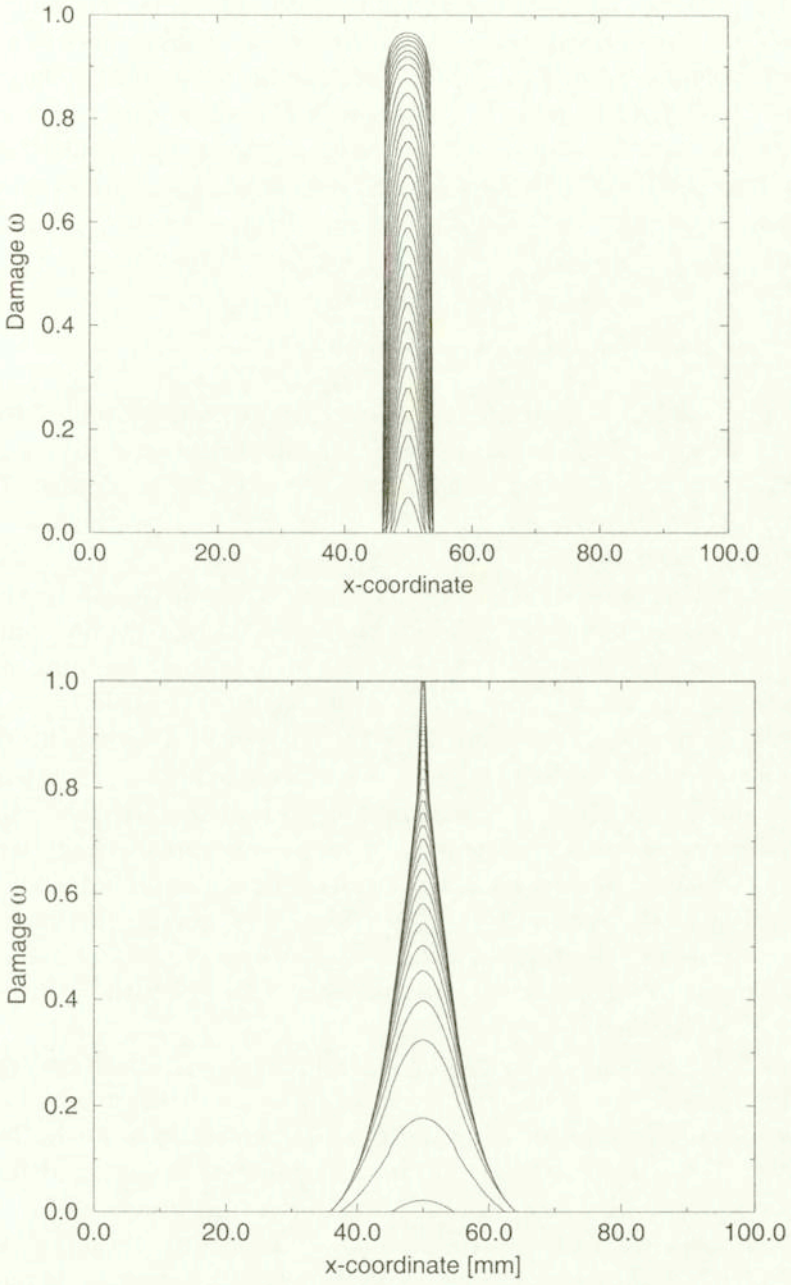

FIG. 6. Damage evolution for hardening gradient plasticity coupled to (a) damage with the damage law representing linear softening, and (b) linear damage. The damage threshold $\kappa_o = 0.0001$.

in the imperfect part of the bar and then, due to hardening, a plastic state is reached in the whole bar. However, once damage starts, softening is observed and localization of both damage and plastic processes takes place in a zone whose size and evolution depend on the damage law and threshold as shown in Fig. 6. For $\kappa_o = 0.0001$ a fast growth of damage is first observed in two central finite elements and then the damage zone gradually expands. The regularization related to plasticity seems to be active for the softening caused by damage, see also [23]. However, the predicted stiffness degradation is again unrealistically small (Fig. 5b).

6.2. Gradient damage coupled to hardening plasticity

We now consider the case of gradient damage theory coupled to hardening plasticity. The length of the bar, the size of the imperfection and Young's modulus are the same as before. The gradient constant $c = 1$ mm^2 is adopted. The damage growth function representing linear softening, Eq. (5.5), with $\kappa_o = 0.0001$ and $\kappa_u = 0.0125$ is employed.

The strain measure is either the total strain $\tilde{\epsilon} = \epsilon$ or the elastic strain $\tilde{\epsilon} = \epsilon^e$. In Figs. 7–8 the solutions obtained for pure gradient damage are compared with the two combinations with hardening plasticity. Now, the beginning of the plastic process is slightly delayed with respect to the damage threshold ($\sigma_y = 5$ N/mm^2).

Figure 7a shows a comparison of load-displacement diagrams for different values of the hardening modulus h. For $\tilde{\epsilon} = \epsilon$ the coupled model gives a more brittle response and for $\tilde{\epsilon} = \epsilon^e$ the results show an increased ductility. The value adopted in this test for the hardening modulus h may seem unrealistically large, but we note that plasticity now represents the behaviour of the material "skeleton" (the fictitious body, see Section 2) and the evolution of microcracks and microvoids which causes the strength and stiffness degradation of the material is modelled by the damage component. For an increasing value of h the solution for pure damage is approached.

Figure 7b compares the unloading branches for $h = E$. Both combined models result in irreversible strains. If the strain measure is based on elastic strains, damage evolution is governed by the effective stress. This is why for this case and for pure damage, the same stiffness degradation is observed for the same stress level. However, a large irreversible strain is now present.

The damage evolution for the two damage measures and $h = E$ is shown in Fig. 8. For $\tilde{\epsilon} = \epsilon^e$ the obtained damage evolution is the same as for pure gradient damage. This is because plasticity and damage contribute to the response without mutual interaction. For $\tilde{\epsilon} = \epsilon$ no further expansion of the damage zone is observed after the plastic process has started, so the solution is more localized.

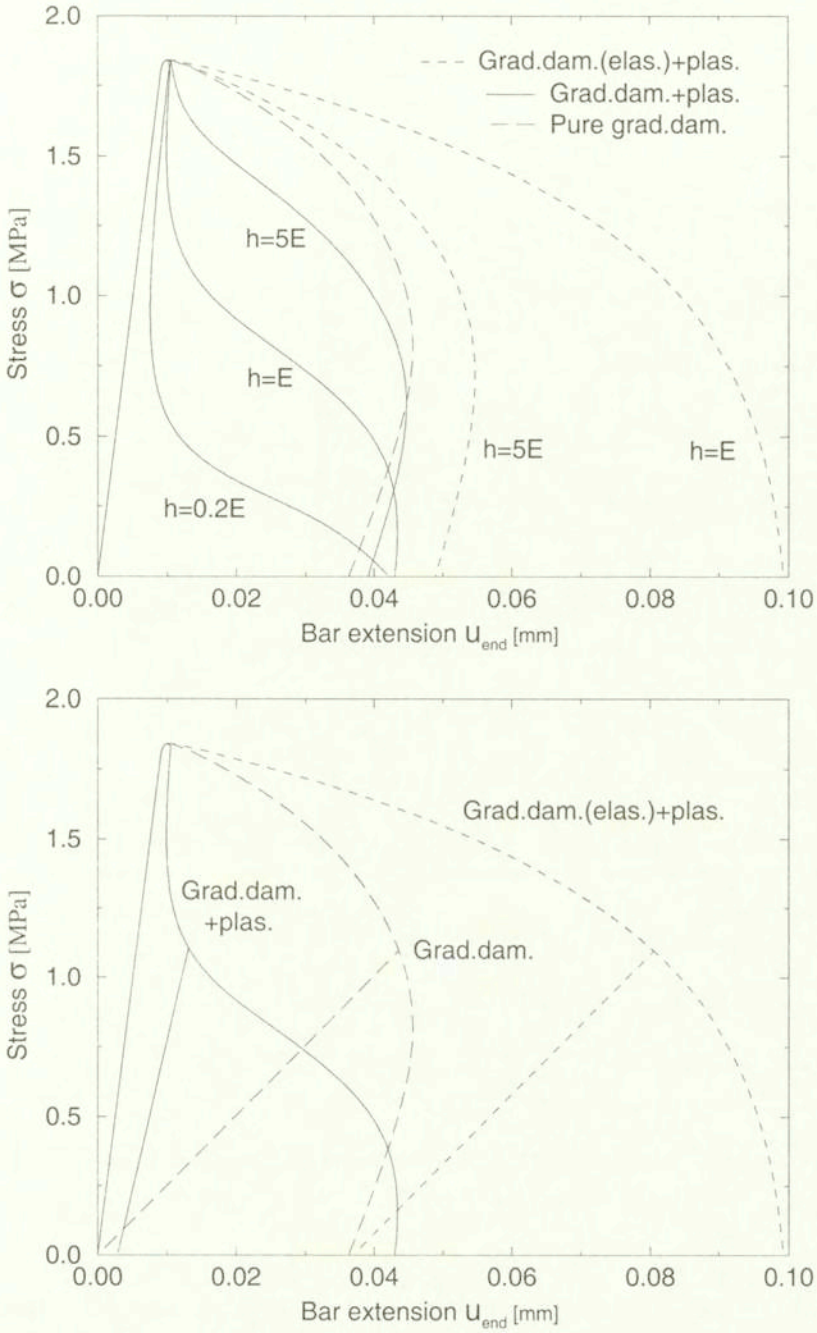

FIG. 7. Gradient damage combined with plasticity ($c = 1$ mm^2): (a) sensitivity of load-displacement diagrams to hardening modulus h, (b) unloading stiffness for damage measure based on total and elastic strains.

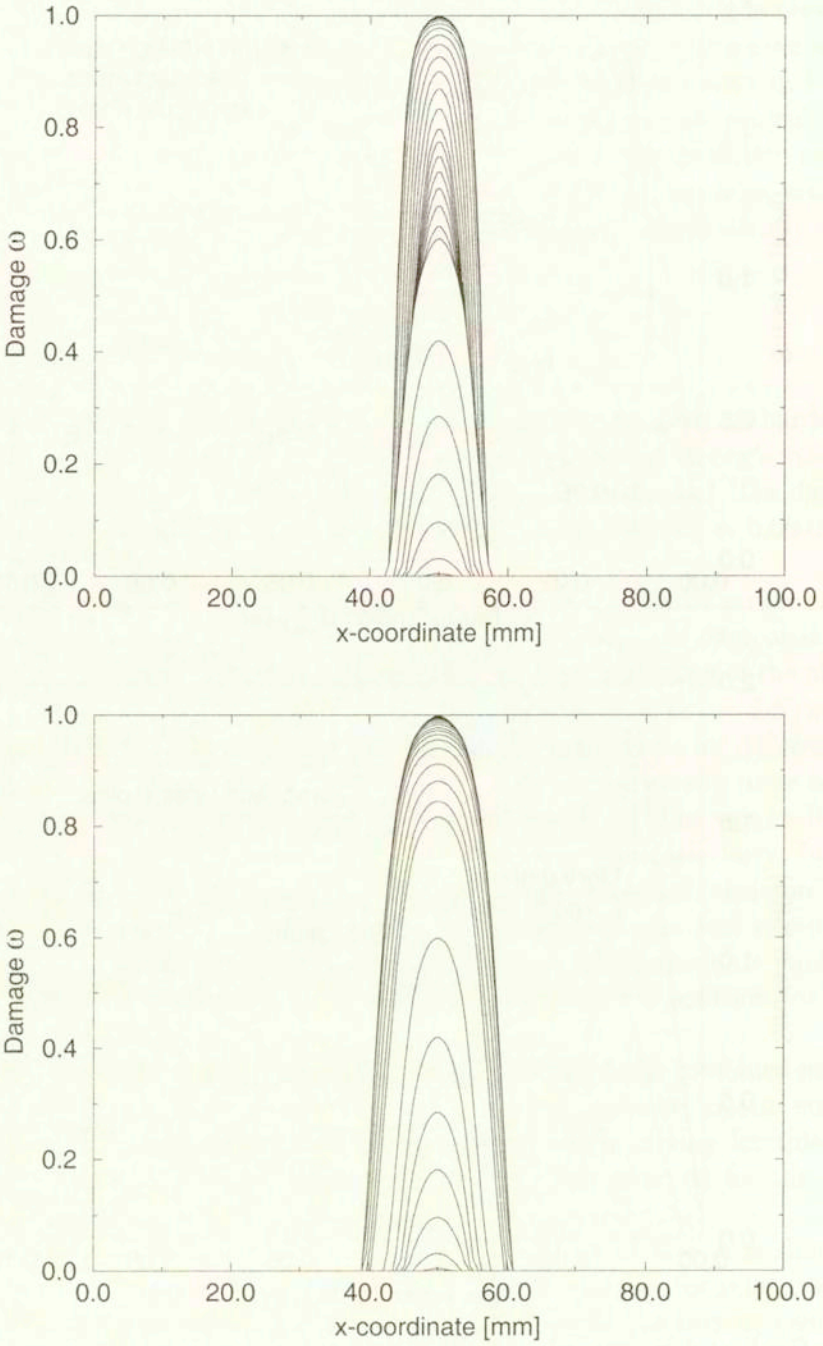

FIG. 8. Damage evolution for (a) gradient damage with total strain measure $\tilde{\epsilon} = \epsilon$ and (b) gradient damage with elastic strain measure $\tilde{\epsilon} = \epsilon^e$. Gradient factor $c = 1$ mm^2.

The only unstable part of the constitutive model, i.e. the damage growth, is regularized by the gradient enhancement, so the results do not exhibit spurious mesh sensitivity [17].

7. Four-point bending test

The four-point bending test is a plane-stress simply-supported beam configuration which has been used in standard experiments of concrete fracture under monotonic and reversed loading in [27]. A symmetric half of the original specimen is shown in Fig. 9 together with the finite element mesh employed in the present computations. The thickness of the beam is 50 mm. The vertical force is exerted under deformation control.

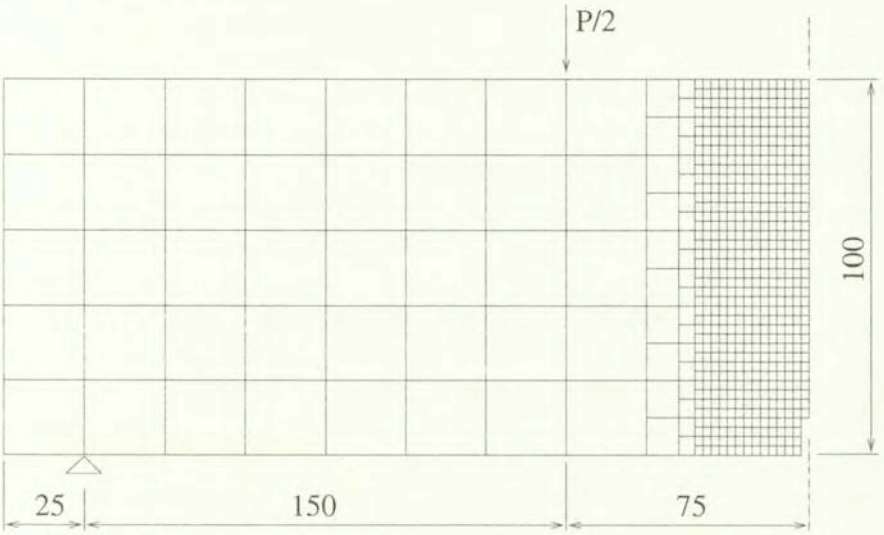

FIG. 9. Four-point bending test – discretized configuration (dimensions in mm).

Four cases have been analyzed: pure gradient damage, gradient damage coupled to plasticity by the equivalent strain measure based on total strains $\tilde{\epsilon}(\boldsymbol{\epsilon})$, the gradient damage-plasticity with damage driven by elastic strains $\tilde{\epsilon}(\boldsymbol{\epsilon}^{\mathrm{e}})$ and, finally, pure gradient plasticity. Although the softening gradient plasticity with the Rankine failure function, i.e. when $\tilde{\sigma}$ in Eq. (3.1) is the maximum principal stress, is capable of reproducing to some extent the decohesive material failure which usually underlies damage [20, 28], the lack of elastic stiffness degradation makes the model unacceptable for cyclic loading. However, coupling of this theory to damage pursued in Sec. 6.1 suffers from three drawbacks: the predicted stiffness degradation is too small, the results are excessively sensitive to the damage threshold [17], and, more importantly, it is difficult to find physical grounds for

a combination of two softening mechanisms even if the regularization of only the plastic component of the model leads to mesh-insensitive results. Therefore, this coupled model will not be used here.

For gradient damage coupled to plasticity the Huber-von Mises criterion has served as the yield function. However, the Drucker-Prager plasticity theory can also be used in the combined model if the difference between the uniaxial and biaxial compressive strength and the possible non-normality of plastic flow become important. The modified von Mises definition of the equivalent strain measure from Eq. (5.2) with $k = 10$ and the exponential damage law from Eq. (5.6) have been used, cf. [29].

The following model parameters have been adopted: Young's modulus $E = 40000$ N/mm^2, Poisson's ratio $\nu = 0.20$, damage threshold $\kappa_o = 0.000075$, damage growth function parameters $\alpha = 0.92$, $\eta = 300$, yield strength $\sigma_y = 4.5$ N/mm^2, hardening modulus $h = E/2$, gradient influence factor $c = 4$ mm^2. The value of σ_y is chosen such that the damage and plastic processes commence almost simultaneously. Gradient damage elements with quadratic interpolation of displacements, linear interpolation of the averaged strain measure, and 2×2 Gauss integration have been employed [21].

For pure gradient plasticity the Rankine failure function has been used with the exponential softening law $\sigma_y(\kappa^p)$ of CORNELISSEN, HORDIJK and REINHARDT [27]. The following model parameters have been adopted: Young's modulus as above, Poisson's ratio $\nu = 0$, uniaxial tensile strength $f_t = 3.0$ N/mm^2, fracture energy $G_f = 0.125$ Nmm/mm^2. The gradient influence factor g is assumed to decrease with the increase of the equivalent inelastic strain measure $g = -l^2\sigma_y'(\kappa^p)$, cf. [20], and an internal length scale $l = 3$ mm is adopted. Gradient plasticity elements with quadratic interpolation of displacements, Hermitean interpolation of the plastic multiplier and reduced Gauss integration (2×2) have been employed [20].

In Fig. 10 the computed load-displacement diagrams are compared. The deflection v is measured at midspan at the bottom of the beam. It is first observed that, with the adopted parameters, the diagrams for Rankine gradient plasticity and pure gradient damage coincide rather closely. However, the response in unloading is far from reality. In loading, a more brittle response is observed for gradient damage coupled to damage through $\tilde{\epsilon}(\boldsymbol{\epsilon})$, while for $\tilde{\epsilon}(\boldsymbol{\epsilon}^e)$ a larger ductility is obtained, since damage is then a function of elastic strains which grow much slower during the plastic process.

Figure 11 shows the incremental deformation pattern obtained for the pure gradient plasticity and gradient damage models at the final points on the curves in Fig. 10. It is observed that in both cases localization appears in a zone broader than one row of elements. It is also noticed that while for the gradient-damage model a quadratic convergence of the incremental-iterative algorithm is

observed, for gradient plasticity the convergence is slow due to problems with the satisfaction of the weak form of the yield condition $(3.2)_2$ at the notch.

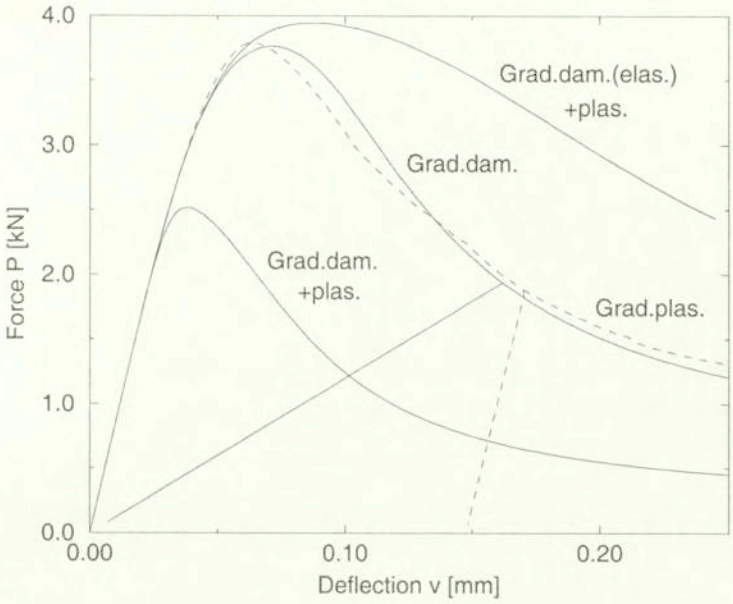

FIG. 10. Load-displacement diagrams for four-point bending test (gradient plasticity diagram dashed).

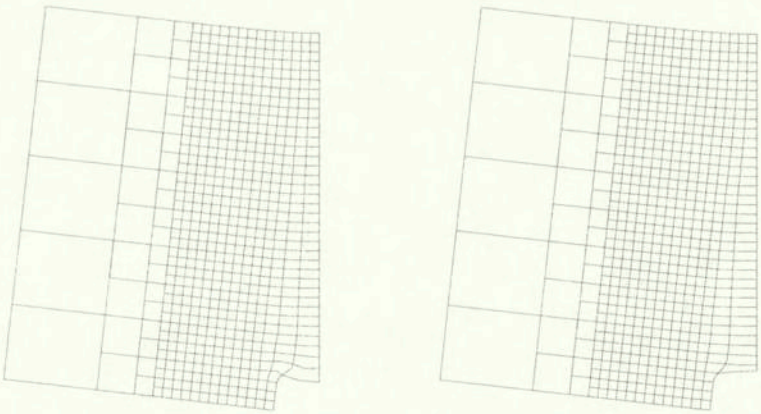

FIG. 11. Four-point bending: final displacement pattern in the central zone for (a) gradient plasticity and (b) for pure gradient damage.

As shown in Figs. 12–13 the two gradient damage-plasticity models can easily be tuned to fit the experimental results of [27]. The crucial point is that for both damage-plasticity combinations, the load reversals exhibit a proper gradual in-

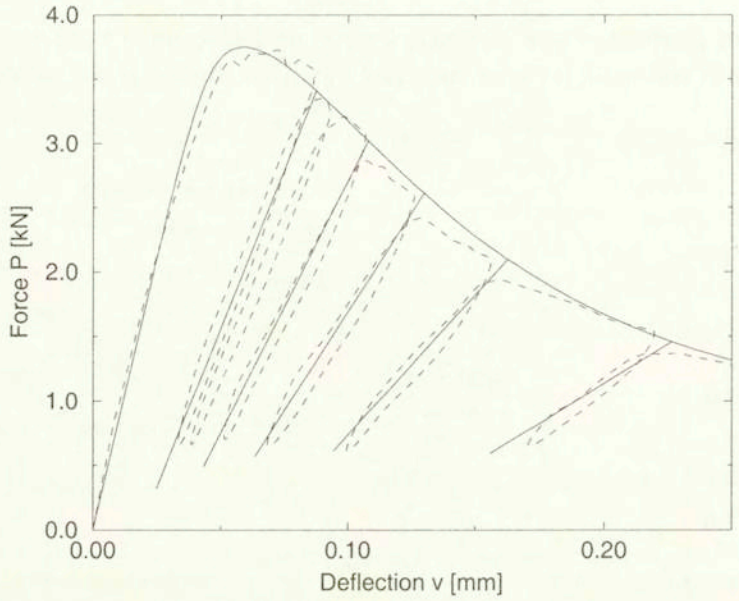

FIG. 12. Experimental and simulated load-displacement diagrams – gradient damage coupled to plasticity $\tilde{\epsilon}(\epsilon)$. Model parameters: $c = 4$ mm^2, $\sigma_y = 6.5$ N/mm^2, $h = E/2$, $\kappa_o = 0.00011$, $\alpha = 0.90$, $\eta = 160$.

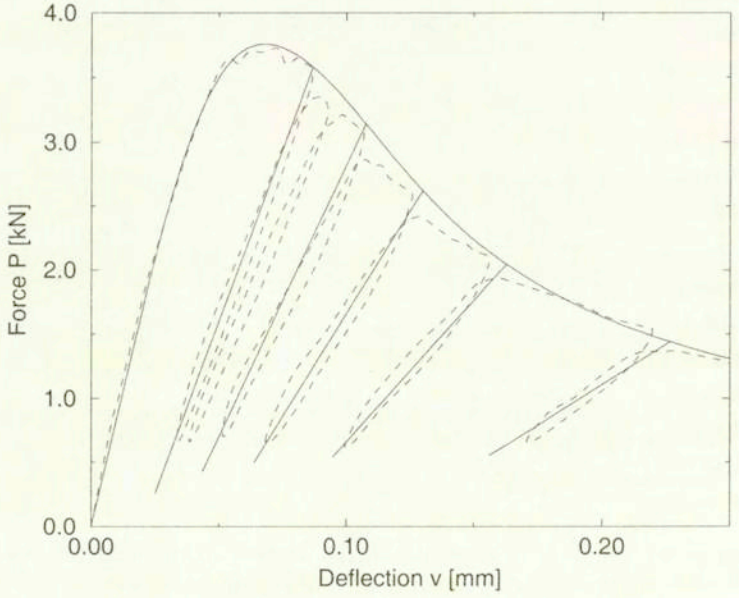

FIG. 13. Experimental and simulated load-displacement diagrams – gradient damage with plasticity $\tilde{\epsilon}(\epsilon^e)$. Model parameters: $c = 4$ mm^2, $\sigma_y = 4.5$ N/mm^2, $h = E/2$, $\kappa_o = 0.00008$, $\alpha = 0.92$, $\eta = 600$.

crease of elastic stiffness degradation. However, the hysteretic loops observed in the experiment can not be reproduced with the present model. To achieve this, the plasticity model must be augmented by a kinematic hardening and the damage description must be split into parts related to positive and negative strains, see for instance [6, 8]. This would also allow for a simulation of crack closure effects. Another solution may be to enhance a generalized plasticity model like that shown in [30] with a localization limiter.

Finally, Fig. 14 presents the damage zone, the averaged strain distribution and the equivalent plastic strains distribution for gradient damage coupled to plasticity. The results are plotted for the final point on the computed load-displacement diagram in Fig. 12. We observe that the averaged and, especially, plastic strains are much more localized than the damage distribution.

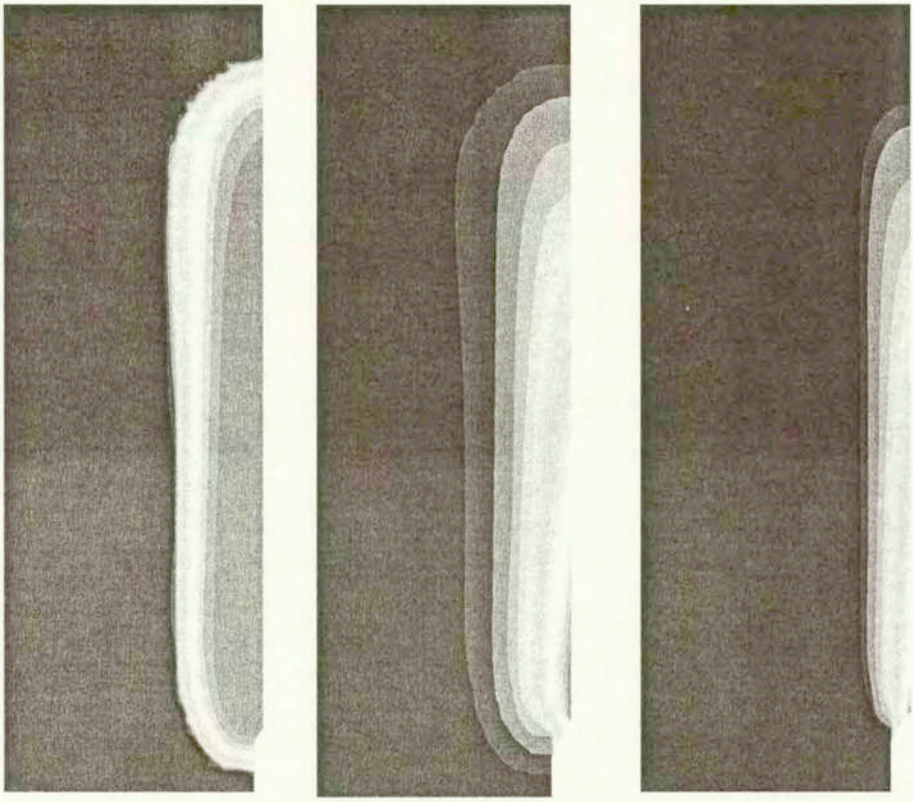

FIG. 14. Fracture zone of four-point bending test: (a) final damage distribution, (b) averaged strain and (c) equivalent plastic strain distribution for gradient damage based on total strains.

As has been noticed in [22], the damage predictions of the model with a constant gradient influence factor c and the exponential damage evolution law may be unrealistic for two-dimensional configurations, since the damage zone tends to broaden instead of evolving into a crack when failure is approached. The coupling to plasticity does not solve this problem. If a localized final damage pattern is to be simulated, the gradient-damage model must be improved, for instance by making the gradient influence factor variable and adopting a different damage law, see [22].

8. Final remarks

Plasticity and damage theories are both capable of reproducing the experimental load-displacement diagrams obtained for quasi-brittle materials under monotonic loading. However, since strain softening and localization are involved, the models must be regularized. To reproduce a realistic stiffness degradation and get closer to a proper modelling of damaging or fracture processes, a combination of the two theories is proposed. It seems that a compromise must be made between a sophisticated modelling of constitutive properties like anisotropic damage and a proper treatment of ill-posedness problems. In this paper a higher weight has been attributed to the latter issue while the constitutive description retains a rather simple, isotropic format. This obviously limits its applicability, although the use of concepts as the modified von Mises equivalent strain measure allows to incorporate the difference of the response to tensile and compressive forces. As also shown in [29], this leads to quite realistic fracture simulations in concrete.

Two types of gradient-dependent couplings of plasticity and damage have been summarized. They are formulated is such a way that the coupling influences only the equilibrium equations, while the second differential equation, which serves the purpose of regularization, preserves the original format of gradient plasticity [19] and gradient damage [21], respectively. For both couplings, consistently linearized two-field finite element formulations have been used [17].

The combination of softening gradient plasticity with damage, in spite of being considered in the numerical experiments, does not seem to have a good physical motivation. The combination of hardening gradient plasticity with damage, considered here and also in a slightly different form in [23], has the weakness that the attachment of the regularization procedure to a hardening plasticity model raises doubts. As shown in [17], these models also seem to suffer from an excessive sensitivity to the damage threshold.

On the other hand, the combination of gradient damage with hardening plasticity gives promising results: the physical interpretation of the model components is convincing, there are few model parameters to be determined, the elastic stiffness degradation is properly reproduced and spurious mesh sensitivity of re-

sults is avoided [17]. Although the fully coupled model with a strain measure based on total strains has a better physical background, no clear evidence has been found that the coupling based on an elastic strain measure should be discarded.

Acknowledgments

Valuable discussions on gradient damage with Dr M.G.D. GEERS from the Eindhoven University of Technology/Royal Military Academy, Brussels are gratefully acknowledged. Financial support of the von Humboldt Foundation and the Max-Planck Society through the Max-Planck Research Award 1996 to the second author and of the Polish Committee for Scientific Research (grant PB 7 T07A 03612) to the first author are gratefully acknowledged.

References

1. J.W. DOUGILL, *Some remarks on path independence in the small in plasticity*, Qt. Appl. Math., **32**, 233–243, 1975.
2. Y.F. DAFALIAS, *Elasto-plastic coupling within a thermodynamic strain space formulation of plasticity*, Int. J. Non-Linear Mechanics, **12**, 327–337, 1977.
3. G. MAIER and T. HUECKEL, *Nonassociated and coupled flow rules of elastoplasticity for rock-like materials*, Int. J. Rock Mech. Min. Sci. & Geomech. Abstr., **16**, 77–92, 1979.
4. Z.P. BAŽANT and S.S. KIM, *Plastic-fracturing theory for concrete*, ASCE J. Eng. Mech., **105**(3), 407–421, 1979.
5. A. DRAGON and Z. MRÓZ, *A continuum theory for plastic-brittle behaviour of rock and concrete*, Int. J. Engng Sci., **17**(2), 121–137, 1979.
6. M. ORTIZ, *A constitutive theory for the inelastic behaviour of concrete*, Mechanics of Materials, **4**, 67–93, 1985.
7. J.C. SIMO and J.W. JU, *Strain- and stress-based continuum damage models – I. Formulation, II. Computational aspects*, Int. J. Sol. Struct., **23**(7), 821–869, 1987.
8. J.W. JU, *On energy-based coupled elastoplastic damage theories: constitutive modeling and computational aspects*, Int. J. Sol. Struct., **25**(7), 803–833, 1989.
9. N.R. HANSEN and H.L. SCHREYER, *A thermodynamically consistent framework for theories of elastoplasticity coupled with damage*, Int. J. Sol. Struct., **31**(3), 359–389, 1994.
10. I. DOGHRI, *Numerical implementation and analysis of a class of metal plasticity models coupled with ductile damage*, Int. J. Num. Meth. Eng., **38**, 3403–3431, 1995.
11. F. MAROTTI de SCIARRA, *General theory of damage elastoplastic models*, ASCE J. Eng. Mech., **123**(10), 10003–1011, 1997.
12. R. DE BORST and E. VAN DER GIESSEN, *Material instabilities in solids*, IUTAM, John Wiley & Sons, Chichester 1998.
13. Z.P. BAŽANT and G. PIJAUDIER-CABOT, *Nonlocal continuum damage, localization instability and convergence*, ASME J. Appl. Mech., **55**, 287–293, 1988.

14. L.J. SLUYS, *Wave propagation, localization and dispersion in softening solids*, Ph. D. disseration, Delft University of Technology, Delft 1992.

15. R. DE BORST, L.J. SLUYS, H.-B. MÜHLHAUS, and J. PAMIN, *Fundamental issues in finite element analyses of localization of deformation*, Eng. Comput., **10**, 99–121, 1993.

16. R. DE BORST, J. PAMIN, R.H.J. PEERLINGS, and L.J. SLUYS, *On gradient-enhanced damage and plasticity models for failure in quasi-brittle and frictional materials*, Computational Mechanics, **17**, 130–141, 1995.

17. R. DE BORST, J. PAMIN, and M.G.D. GEERS, *On coupled gradient-dependent plasticity and damage theories with a view to localization analysis*, Eur. J. Mech.: A/Solids, 1999. Accepted for publication.

18. H.-B. MÜHLHAUS and E.C. AIFANTIS, *A variational principle for gradient plasticity*, Int. J. Sol. Struct., **28**, 845–857, 1991.

19. R. DE BORST and H.-B. MÜHLHAUS, *Gradient-dependent plasticity: Formulation and algorithmic aspects*, Int. J. Num. Meth. Eng., **35**, 521–539, 1992.

20. J. PAMIN, *Gradient-dependent plasticity in numerical simulation of localization phenomena*, Ph. D. dissertation, Delft University of Techology, Delft 1994.

21. R.H.J. PEERLINGS, R. DE BORST, W.A.M. BREKELMANS, and J.H.P. DE VREE, *Gradient-enhanced damage for quasi-brittle materials*, Int. J. Num. Meth. Eng., **39**, 3391–3403, 1996.

22. M.G.D. GEERS, *Experimental analysis and computational modelling of damage and fracture*, Ph. D. dissertation, Eindhoven University of Technology, Eindhoven 1997.

23. T. SVEDBERG and K. RUNESSON, *A thermodynamically consistent theory of gradient-regularized plasticity coupled to damage*, Int. J. Plasticity, **13**(6-7), 669–696, 1997.

24. R. HILL, *A general theory of uniqueness and stability in elastic-plastic solids*, J. Mech. Phys. Solids, **6**, 236–249, 1958.

25. J. MAZARS and G. PIJAUDIER-CABOT, *Continuum damage theory – application to concrete*, ASCE J. Eng. Mech., **115**, 345–365, 1989.

26. J.H.P. DE VREE, W.A.M. BREKELMANS, and M.A.J. VAN GILS, *Comparison of nonlocal approaches in continuum damage mechanics*, Comp. & Struct., **55**(4):581–588, 1995.

27. D.A. HORDIJK, *Local approach to fatigue of concrete*, Ph. D. dissertation, Delf University of Technology, Delft 1991.

28. R. DE BORST and J. PAMIN, *Gradient plasticity in numerical simulation of concrete cracking*, Eur. J. Mech.: A/Solids, **15**:295–320, 1996.

29. R.H.J. PEERLINGS, R. DE BORST, W.A.M. BREKELMANS, and M.G.D. GEERS, *Gradient-enhanced damage modelling of concrete fracture*, Mech. Cohes.-frict. Mater., **3**:323–342, 1998.

30. A. WINNICKI and CZ. CICHOŃ, *Plastic model for concrete in plane stress state. I: Theory, II: Numerical validation*, ASCE J. Eng. Mech., **124**(6), 591–602, 603–613, 1998.

Received December 23, 1999; new version May 5, 1999.